

Investigation on Viscosity and Nonisothermal Crystallization Behavior of P-Bearing Steelmaking Slags with Varying TiO₂ Content



ZHANJUN WANG, YONGQI SUN, SEETHARAMAN SRIDRAR, MEI ZHANG,
and ZUOTAI ZHANG

The viscous flow and crystallization behavior of CaO-SiO₂-MgO-Al₂O₃-Fe_tO-P₂O₅-TiO₂ steelmaking slags have been investigated over a wide range of temperatures under Ar (High purity, >99.999 pct) atmosphere, and the relationship between viscosity and structure was determined. The results indicated that the viscosity of the slags slightly decreased with increasing TiO₂ content. The constructed nonisothermal continuous cooling transformation (CCT) diagrams revealed that the addition of TiO₂ lowered the crystallization temperature. This can mainly be ascribed to that addition of TiO₂ promotes the formation of [TiO₆]-octahedra units and, consequently, the formation of MgFe₂O₄-Mg₂TiO₄ solid solution. Moreover, the decreasing viscosity has a significant effect on enhancing the diffusion of ion units, such as Ca²⁺ and [TiO₄]-tetrahedra, from bulk melts to the crystal-melt interface. The crystallization of CaTiO₃ and CaSiTiO₅ was consequently accelerated, which can improve the phosphorus content in P-enriched phase (*n*2CaO·SiO₂-3CaO·P₂O₅). Finally, the nonisothermal crystallization kinetics was characterized and the activation energy for the primary crystal growth was derived such that the activation energy increases from -265.93 to -185.41 KJ·mol⁻¹ with the addition of TiO₂ content, suggesting that TiO₂ lowered the tendency for the slags to crystallize.

DOI: 10.1007/s11663-016-0825-4

© The Minerals, Metals & Materials Society and ASM International 2016

I. INTRODUCTION

THE production of crude steel in China surpassed 800 million tons in 2015, disposing nearly 80 to 100 million tons of steelmaking slags.^[1] Nevertheless, only about 30 wt pct of steelmaking slags were recycled as construction materials, soil conditioners, fertilizers, recovery of metals or recovered in iron- and steelmaking process, *etc.*^[2-7] Among these utilization methods, the most effective way of using the steelmaking slags was recycled into the iron- and steelmaking process, which may inevitably result in the enrichment of phosphorus in the slags and further increase the burden in the following dephosphorization process.^[8-10] Thus, the lowering of the phosphorus content in steelmaking slags is of primary concern for further utilization of P-bearing steelmaking slags. The selective crystallization and phase separation (SCPS) method has been proved to

be the most efficient way to recycle the phosphorous in steelmaking slags.^[11-13] During the SCPS process, the selective crystallization is the key step to enrich phosphorous successfully into a certain phase, which can be separated and used as phosphorus fertilizer, and the residues may be recycled into the iron- and steelmaking process.

During the early 1960s and 1980s, several investigations were conducted to detect the dephosphorization process.^[14-17] These investigations were mainly based on the CaO-SiO₂-Fe_tO-P₂O₅ system to study the mechanism of dephosphorization, and the *n*(2CaO·SiO₂-3CaO·P₂O₅) (*n*C₂S-C₃P) solid solution was considered to be the efficient P-enriched phase. Based on these investigations, various studies have been explored to reveal how to boost the phosphorus content in *n*C₂S-C₃P solid solution through adding different additives into the complex CaO-SiO₂-MgO-Al₂O₃-Fe_tO-P₂O₅ multiphase.^[9,18-21] A series of studies has been carried out to explore the P concentrating phase in steelmaking slags modified by Fe₂O₃, P₂O₅, Al₂O₃, and CaF₂ additives,^[22-25] where the essential structure of the slags has been systematically studied, especially Fe³⁺, P⁵⁺, Al³⁺, and F⁻. Meanwhile, some other studies about the structure also replenished the investigation of the slags.^[26-29] Nevertheless, the existing data are still too limited to cover all of the slag compositions. Some studies showed that TiO₂ can also be used as an additive to improve P (or V) solid solubility in the P (or V)-enriched phase,^[19,30] during which process the viscosity and crystallization ability changed

ZHANJUN WANG, Doctoral Candidate, and MEI ZHANG, Professor, are with the School of Metallurgical and Ecological Engineering, University of Science and Technology Beijing, 100083 Beijing, P.R. China. YONGQI SUN, Doctoral Candidate, is with the College of Engineering, Peking University, 100871 Beijing, P.R. China. SEETHARAMAN SRIDRAR, Professor, is with the Advanced Steel Research Centre, WMG, Steels Processing Research Centre, University of Warwick, Coventry CV4 7AL, U.K. ZUOTAI ZHANG, Professor, is with the School of Environmental Science and Engineering, South University of Science and Technology of China, 518055 Shenzhen, P.R. China. Contact e-mail: zhangzt@sustc.edu.cn

Manuscript submitted July 19, 2016.

Article published online October 24, 2016.

correspondingly. It is well known that Ti^{4+} can act as a network former cation with fourfold coordination of oxygen or a network modifier cation with sixfold coordination of oxygen. The effect of TiO_2 on enrichment of phosphorus was strongly needed for systematic extrapolation to expand the previous experimental data.

The objective of the present study was to provide a comprehensive exploration and discussion of $\text{CaO-SiO}_2\text{-Al}_2\text{O}_3\text{-MgO-Fe}_t\text{O-P}_2\text{O}_5$ slags modified by TiO_2 with the content range from 0 to 10 wt pct, including the variation of viscosity and structure of the melts, the precipitation sequence of the crystals, and the kinetics of the primary crystals during the continuous cooling.

II. EXPERIMENTAL

The raw materials of the synthetic slags were analytical grade CaO , SiO_2 , MgO , Al_2O_3 , Fe_2O_3 , P_2O_5 , and TiO_2 . The samples were prepared at 1823 K (1550 °C) under 0.3 L/min of Ar (High purity, >99.999 pct) in a platinum crucible to obtain the homogeneous slags for 2 hours. The molten slags were then quenched into water rapidly and crushed for the primary experiments. The quenched slags were examined by X-ray diffraction (XRD) to ensure the glassy phase, as shown in Figure 1. The chemical compositions of the premelted slags for the current study were analyzed by X-ray fluorescence, as shown in Table I, where $\text{Fe}^{3+}/\sum\text{Fe}$ were determined by the titration method. Additionally, the equilibrium state of the molten slag can be achieved when the holding time was beyond 2 hours. It can be clarified through the constant $\text{Fe}^{3+}/\sum\text{Fe}$ values. It is therefore reasonable to conclude that the premelted slags with the holding time for 2 hours can be used for further measurement.

The viscosity measurement was carried out by a rotating cylinder method using a rotating spindle connected to a calibrated Brookfield digital viscometer

(model LVDV-II+, Brookfield Engineering Laboratories, Middleboro, MA). The experimental apparatus for the viscosity measurement and the other details of the experimental apparatus can be found in our previous study.^[25,31] Within the scope of the viscosity measurement, although the oxygen partial pressure around the Mo crucible was low enough, the Mo crucible was inevitably oxidized as MoO_x . The MoO_x contents after the viscosity were less than 0.71 wt pct, and the change before and after the viscosity measurement is less than 0.32 wt pct. Therefore, the effect of MoO_x can be ignored during the viscosity measurement.

The nonisothermal melt crystallization of the slags was evaluated with a differential scanning calorimeter (DSC) by a SETARAM instrument (Setsys Evolution, S60/58341, SETARAM Instrumentation, France) in Ar atmosphere (Ar purity >99.999 pct) at a flow rate of 60 mL/min with $\alpha\text{-Al}_2\text{O}_3$ as the reference. Before the DSC experiment, the instrument calibration was performed using high-purity metals of Al, Ag, Au, and Ni. Then, about 40-mg slags were heated up at a constant heating rate of 20 K/min in a platinum crucible with a diameter of 5 mm and a height of 8 mm. The molten slags were held at 1823 K (1550 °C) for 5 minutes to homogenize the chemical composition. Subsequently, the slags were cooled at different cooling rates (5, 10, 15, 20, and 25 K/min). Furthermore, the baseline was employed to calibrate the DSC curves for the buoyancy effect.

Since the molten slags after DSC measurements are too small to identify the crystal phases by XRD and SEM, a series of heat treatment experiments was carried out to determine the sequence of crystalline phase precipitation. First, the previous premelted slags were heated to 1823 K (1550 °C) and cooled to the target temperature at a cooling rate of 10 K/min. Afterward the slags were held about 30 minutes at each target temperature and then quenched by water. The crystals in slags were identified by XRD and the scanning electronic microscopy equipped with energy-dispersed spectroscopy (SEM/EDS).

A more quantitative analysis of structure can be obtained by using Raman spectra performed with a multichannel modular triple Raman system (JY-HR800, Jobin-Yvon, France) with excitation wavelength of 532 nm and a 1-mW semiconductor laser as the light source. Solid-state ^{29}Si MAS-NMR measurements of the power glasses were recorded on a 400 M FT-NMR spectrometer (Bruker Avance III 400M, Germany) using a MAS probe with 4-mm ZrO_2 rotor and two pairs of Dupont Vespel caps.

III. RESULTS

A. Viscosity Measurement

The effect of TiO_2 addition on the viscosity of the typical basic oxygen $\text{CaO-SiO}_2\text{-Al}_2\text{O}_3\text{-MgO-Fe}_t\text{O-P}_2\text{O}_5$ steelmaking slags at a fixed CaO/SiO_2 ratio of 1.8 is shown in Figure 2. It can be noted that the slag viscosity

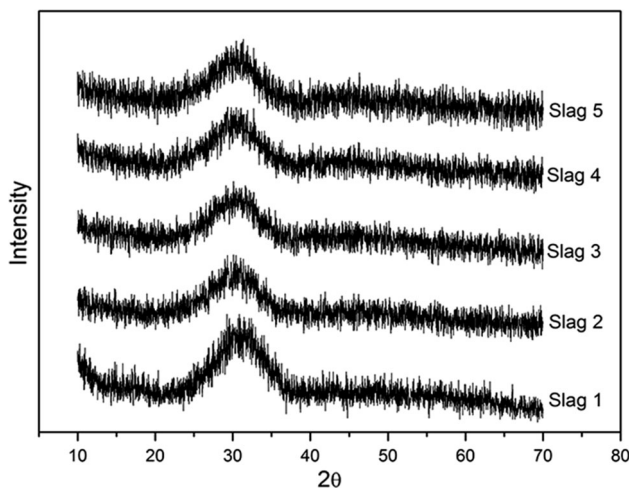


Fig. 1—XRD patterns of different quenched slags at 1823 K (1550 °C).

Table I. Analyses Result of Synthesized Slag Compositions (Weight Percent)

Slag	Basicity	Fe ³⁺ /∑Fe	CaO	SiO ₂	MgO	Al ₂ O ₃	Fe ₂ O	P ₂ O ₅	TiO ₂
1	1.72	0.791	37.81	21.91	6.54	4.85	19.47	9.42	0
2	1.75	0.781	35.51	20.24	6.67	4.85	20.11	9.51	3.11
3	1.79	0.774	34.89	19.46	6.81	4.72	19.87	9.39	4.86
4	1.75	0.791	33.28	18.98	6.91	4.91	19.69	9.54	6.69
5	1.81	0.773	32.26	17.84	6.52	4.69	19.36	9.66	9.67

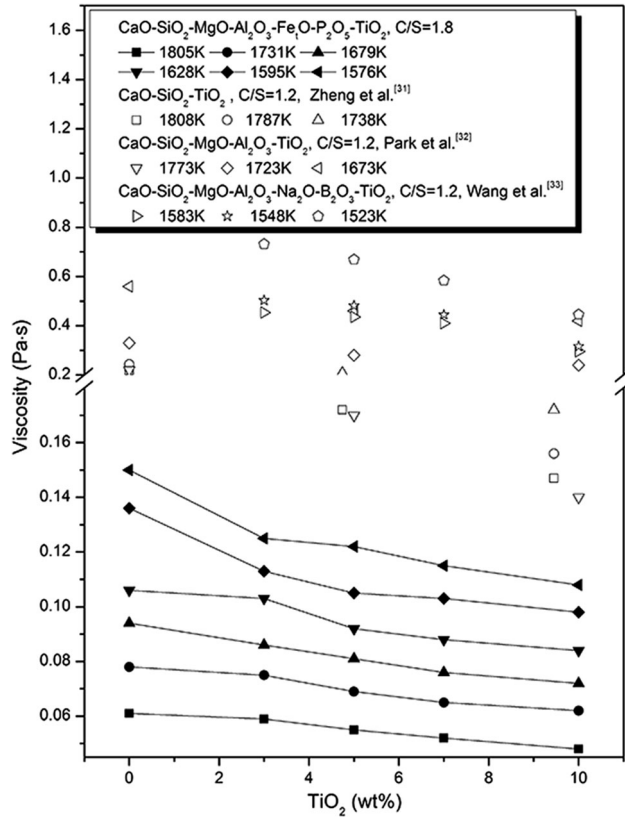


Fig. 2—Effect of TiO₂ on the viscosity of CaO-SiO₂-MgO-Al₂O₃-Fe₂O₃-P₂O₅-(TiO₂) steelmaking slags.

decreases with increasing TiO₂ content. Despite different slag compositions investigated, the variation trend of present results is in good agreement with the previous results. Zheng *et al.*^[31] have investigated the effect of TiO₂ addition on the viscosity of CaO-SiO₂-TiO₂ (C/S = 1.2) slags and found that the viscosity of these ternary slags decreased with an increment in the content of additive TiO₂. Park *et al.*^[32] reported that TiO₂ behaved as the basic oxide and lowered the viscosity in the CaO-SiO₂-Al₂O₃-MgO-based slags by depolymerizing the silicate network structure. Wang *et al.*^[33] examined the effect of TiO₂ addition on the viscosity of the CaO-SiO₂-Al₂O₃-MgO-Na₂O-B₂O₃ system in the temperature range of 1583 K to 1448 K (1310 °C to 1175 °C) and obtained the similar variation trend. Furthermore, the relative viscosity reported by the present study is lower than that of previous investigations, which can be ascribed to the higher basicity and more complex multiphase in the present study.

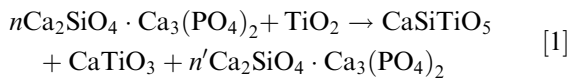
B. DSC Investigation

The DSC investigation of the studied slags was inquired under nonisothermal conditions at five cooling rates. Figure 3 records the DSC curves of the slags with different TiO₂ contents during a continuous cooling process at cooling rates of 5, 10, 15, 20, and 25 K/min, respectively. According to Jung *et al.*,^[26] each separate peak suggested a discrete crystallization of different phases during the cooling process. The starting point of the crystallization (onset temperature, *T*_{onset}) was taken from the intersection between the tangent line of the heat flow curve before the exothermic peak and the tangent line of the steep exothermic peak curve, as shown in Figure 3(a). At all considered cooling rates, the DSC curves of slag 1 have similar shapes; *i.e.*, four DSC exothermic peaks were obtained in Figure 3(a). The peaks were denoted as P1, P2, P3, and P4 for slag 1, corresponding to four different crystallization events that occurred in slag 1 under different continuous cooling rates.^[34] Nevertheless, it was observed that there were five exothermic peaks for slags containing TiO₂, indicating the occurrence of a new crystallization event in the slag with TiO₂ additions. For the TiO₂-containing slags, the peaks were designated as P1, P2, P3, P4, and P5, respectively. Comparing the position of exothermic peaks on DSC curves at the cooling rate of 5 K/min, a significant shift occurred toward a lower temperature and shape of exothermic peaks became sharper with an increasing cooling rate. Clearly, crystallization parameters such as nucleation and growth rates are functions of viscosity and degree of undercooling. Therefore, at a higher cooling rate, a higher undercooling was required and a lower crystallization temperature was caused.

Based on the aforementioned results, the CCT diagrams for the primary crystals with varying TiO₂ contents were constructed. It can be seen from Figure 4 that the crystallization temperature decreases with increasing TiO₂ contents in the slags, which suggests that TiO₂ lowers the tendency of crystallization. This result is not completely consistent with the previous results. For instance, Wen *et al.*^[35] found that the crystallization ability of CaO-SiO₂-TiO₂ systems increased first with increasing TiO₂ content, while the crystallization was restrained with further addition of TiO₂ content. The difference of the crystallization ability can be ascribed to the complex system and the multiple identities of Ti⁴⁺ (network modifier or network former). Therefore, the effect of TiO₂ on crystallization can be further elucidated in the following sections.

C. Identification of the Crystal Phases

To determine the crystal phases associated with the exothermic peaks appearing in the nonisothermal DSC curves, slag 1 and slag 3 were heat treated to qualitative characterize the behavior of crystallization. The slags were melted at 1823 K (1550 °C) and then continuously cooled at the cooling rate of 10 K/min to the desired temperatures. At each desired temperature, the melts would be held 30 minutes isothermally to ensure that the crystal grew to a sufficient size for further characterization, and they were then extracted and quenched in water. The as-quenched slags were analyzed by XRD, and the patterns obtained are shown in Figure 5. It can be seen that MgFe_2O_4 spinel is the first crystal to precipitate upon cooling for slag 1 at 1473 K (1200 °C), followed by MgFe_2O_4 and $n\text{C}_2\text{S-C}_3\text{P}$ that co-precipitated at 1413 K (1140 °C), indicating that the exothermic peaks P1 and P2 represented the precipitation of the spinel (MgFe_2O_4) and the P-enriched phase ($n\text{C}_2\text{S-C}_3\text{P}$), respectively. Unlike slag 1, with increasing TiO_2 content, it can be seen from Figure 5(b) that the first crystalline phase is transformed into the mixture of MgFe_2O_4 and Mg_2TiO_4 . The second exothermic peak P2 still signifies the formation of the P-enriched phase. In addition, it can be seen from the XRD patterns of slag 3 quenched at 1173 K (900 °C) that CaTiO_3 and $\text{Ca}_2\text{TiSiO}_4$ can be detected, which can also be interpreted by the phase diagram of the $\text{CaO-SiO}_2\text{-TiO}_2$ system.^[36] It can be seen from the $\text{CaO-SiO}_2\text{-TiO}_2$ phase diagram that the thermodynamic condition was favorable to the formation of CaTiO_3 and $\text{Ca}_2\text{TiSiO}_4$ at a higher TiO_2 content. For P-bearing slags, the enhancement of CaTiO_3 and $\text{Ca}_2\text{TiSiO}_4$ formation further promoted the enrichment of phosphorus into a certain phase ($n'\text{C}_2\text{S-C}_3\text{P}$, $n > n'$), which would be formulated by the following equation:^[19]



To clarify the XRD results and the morphologies of the crystalline phases, the SEM/EDS technique was employed to display the different types of phases. Figure 6 and Table II show the backscatter electron microscopy of the slags with TiO_2 additions of 0, 5, and 10 wt pct, respectively. It can be seen from Figures 6(a) and (b) that, for slag 1, the first precipitated granular pale crystal can be identified as the spinel (MgFe_2O_4) and the following precipitated polygonal gray crystal can be determined as the P-enriched phase ($n\text{C}_2\text{S-C}_3\text{P}$), respectively. It is worthy to note that the inner part of the polygonal gray crystal (phase C, Figure 6(b)) can be identified as $2\text{CaO}\cdot\text{SiO}_2$. Further consideration about $n\text{C}_2\text{S-C}_3\text{P}$ crystallization behavior and its mechanism would be meaningful. Compared with the previous study, the precipitation mechanism for the P-enriched phase can be elucidated here:^[37] First, $2\text{CaO}\cdot\text{SiO}_2$ particle precipitated from the molten slag; second, P_2O_5 and CaO around the $2\text{CaO}\cdot\text{SiO}_2$ particle diffused to $2\text{CaO}\cdot\text{SiO}_2$ surface quickly; and third, P_2O_5 existed as $3\text{CaO}\cdot\text{P}_2\text{O}_5$ and

diffused into the $2\text{CaO}\cdot\text{SiO}_2$ particle and the composition of the particle changed to $5\text{CaO}\cdot\text{SiO}_2\cdot\text{P}_2\text{O}_5$. As demonstrated in Figure 6(c), for slag 3, the primary crystal transformed to the white lumps. These white lumps cannot be distinguished clearly through the appearance of the crystal, but when combining the image with the XRD and EDS results, the white lumps may be explained as a solid solution of $\text{MgFe}_2\text{O}_4\text{-Mg}_2\text{TiO}_4$.^[38] Furthermore, some other information can also be concluded from the EDS and XRD result that the Fe-enriched phase (MgFe_2O_4) and P-enriched phase ($n\text{C}_2\text{S-C}_3\text{P}$) behaved as the first two precipitated phases during the continuous cooling process.

IV. DISCUSSION

A. Nonisothermal Crystallization Kinetics

With the wide use of DSC to study crystallization, several methods have been put forward to obtain kinetic parameters from nonisothermal experiments carried out at different cooling rates.^[39–41] During the nonisothermal crystallization process, the relative degree of crystallinity can be determined by measuring the partial area of the DSC peak. The relative degree of crystallinity α as a function of relative crystallization time can be theoretically estimated by means of the following equation:^[42]

$$\alpha = \frac{\int_{t_0}^t (dH_t/dt) dt}{\int_{t_0}^{t_1} (dH_t/dt) dt} \quad [2]$$

where dH_t is the measured enthalpy of crystallization during an infinitesimal time interval dt in DSC measurement, t_0 is the time at which the crystallization just begins, and t_1 is the time when the crystallization is completed. Figure 7(a) depicts the relative degree of crystallinity for primary crystal of slag 1 at five different cooling rates, which showed the S-shape curves. It is obviously observed that the t_1 value decreased with increasing cooling rate, suggesting that the crystal grew faster when the cooling rate increased. In addition, the S-shape curves can be schematically divided into three regions, *i.e.*, first the random nucleus of crystal occurring at stage A, then the crystal growing rapidly at stage B, and finally the coalescence of crystal happening at stage C.^[41] Figure 7(b) shows the crystallization time of primary crystals with the cooling rate of 10 K/min. Compared with slag 1, it can be seen that the crystallization time of P1 for slag 2 with 3 wt pct TiO_2 has a slight decrease. This may be attributed to the lower viscosity accelerating the mass transfer. Nevertheless, with the addition of TiO_2 above 3 wt pct, the primary crystal phase is transformed into $\text{MgFe}_2\text{O}_4\text{-Mg}_2\text{TiO}_4$ solid solution. Therefore, the content of the formed solid solution increased with increasing TiO_2 content, resulting in increased crystallization time for $\text{MgFe}_2\text{O}_4\text{-Mg}_2\text{TiO}_4$.

The effect of TiO_2 on the crystallization of the slags was further analyzed by calculating the activation energy of crystal growth, which is one of the most

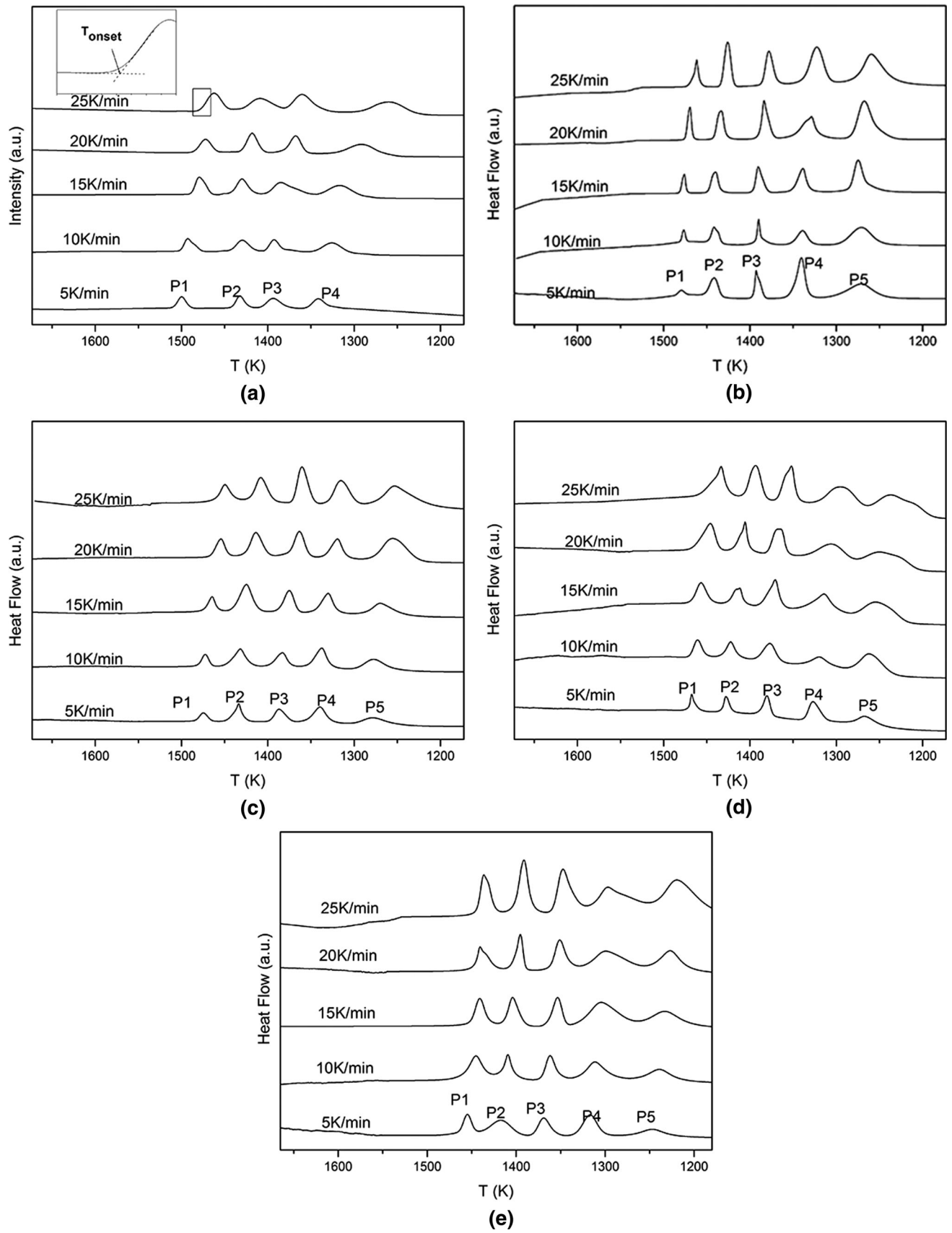


Fig. 3—DSC curves of nonisothermal crystallization of slags at various cooling rates: (a) Slag 1, (b) Slag 2, (c) Slag 3, (d) Slag 4, and (e) Slag 5.

important kinetic parameters for the crystallization process. By taking into account the influence of various cooling rates, Kissinger proposed a method for determining the activation energy values based on the first exothermic crystallization peaks.^[39] In this study, the activation energy E_a could be determined by calculating the variation of the crystallization peak temperature with the cooling rate. The equation was shown as follows:^[39]

$$\ln\left(\frac{\beta}{T_p^2}\right) = -\frac{E_a}{RT_p} + \ln\left(\frac{AR}{E_a}\right) \quad [3]$$

where T_p is the maximum crystallization temperature in a DSC curve, β is the cooling rate, R is the

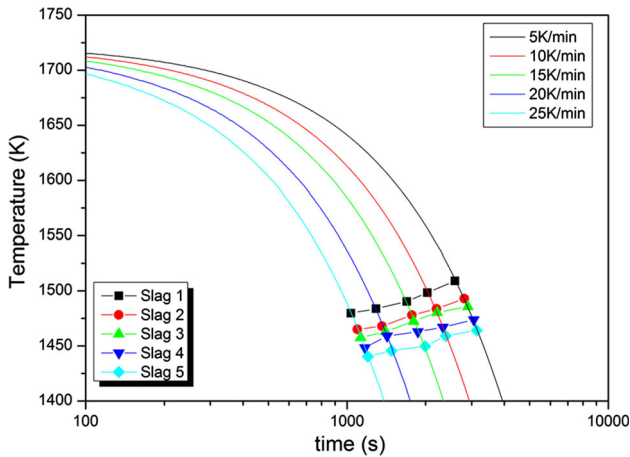


Fig. 4—CCT diagrams of the primary crystal at different TiO_2 contents.

universal gas constant, and A is the frequency factor, respectively. Because the dependence of $\ln(\beta/T_p^2)$ vs $1/T_p$ at considered temperatures is evidently a straight line, it is possible to evaluate the corresponding values of E_a using Eq. [3]. Combined with the slope of the lines, the values of the activation energy were calculated and labeled in Figure 8. It has been assumed in some works that the activation energy can reflect the tendency of the slag to crystallize; *i.e.*, a higher activation energy value means a bigger barrier to form ordered structures.^[43] It can be seen from Figure 8 that, as TiO_2 content increases from 0 to 10 wt pct, there is a noticeable increase on the activation energy for crystal growth. It is suggested that TiO_2 lowers the tendency for the slags to crystallize, which is consistent with the CCT diagrams; *i.e.*, a higher TiO_2 content caused a lower crystallization temperature.

B. Structural Analysis

Generally, the structure characteristic of the slags is closely related to the viscosity and further the crystallization behavior. Therefore, Raman and NMR spectra were employed to detect a clear view of the influence of TiO_2 on the relationship between the viscosity and the crystal formation.

Figure 9 exhibits the deconvoluted Raman spectra of slags 1, 3, and 5, in which the fitting process was conducted under the guidance of the study performed by Mysen.^[44] The previous study assigned the bands at about 855, 920, 988, and 1050 cm^{-1} to the presence of Q^0 , Q^1 , Q^2 , and Q^3 units (Q^n , $n = \text{NBO/Si}$, NBO is the nonbridging oxygen number), respectively. In addition, the peaks near 970 and 1100 cm^{-1} correspond to the

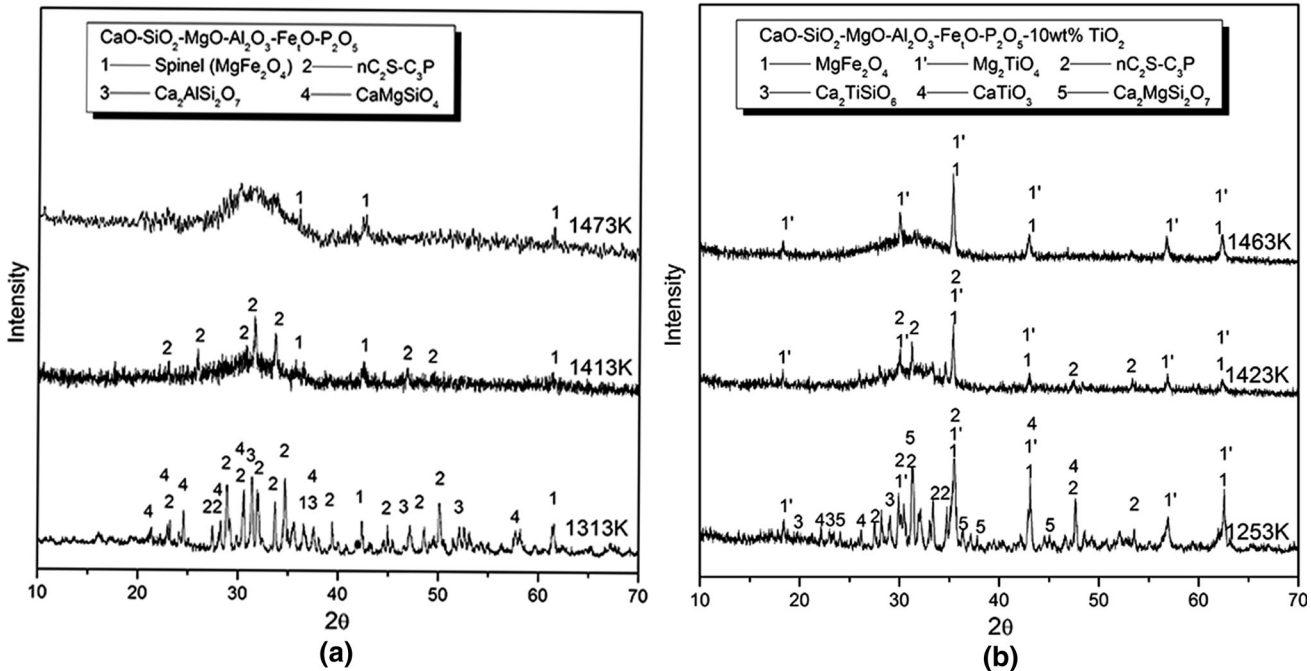


Fig. 5—(a) XRD results of slag 1 quenched at 1473 K, 1413 K, and 1313 K (1200 °C, 1140 °C, and 1040 °C). (b) XRD results of slag 3 quenched at 1463 K, 1423 K, and 1253 K (1190 °C, 1150 °C, and 980 °C).

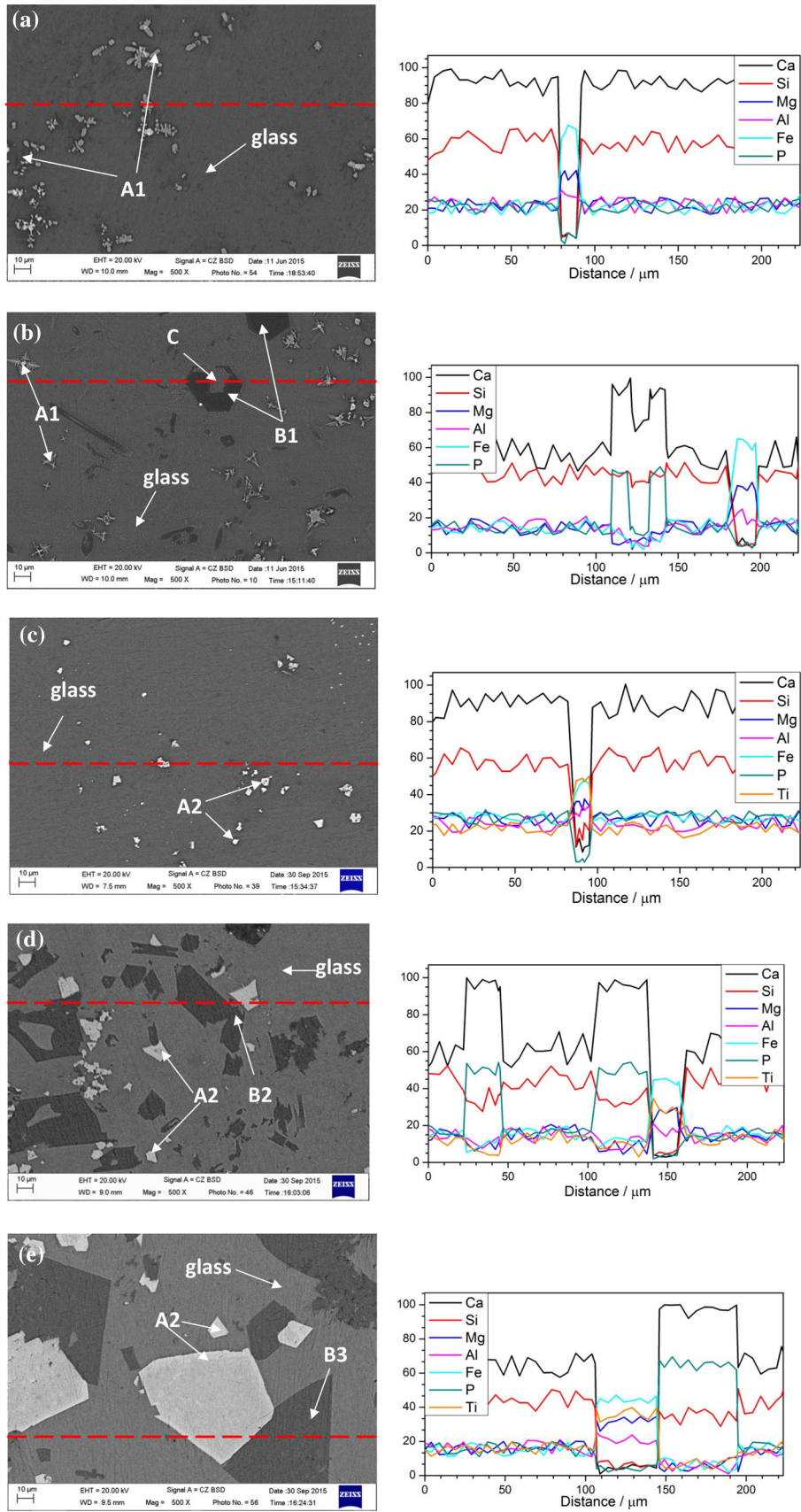


Fig. 6—BSE images and EDS result of slags at the cooling rate of 10 K/min and quenched at corresponding temperatures: (a) Slag 1 at 1473 K (1200 °C), (b) Slag 1 at 1413 K (1140 °C), (c) Slag 3 at 1463 K (1190 °C), (d) Slag 2 at 1423 K (1150 °C), and (e) Slag 5 at 1403 K (1130 °C).

Table II. Results of EDS Analysis of P-Enriched Phase for Slags 1, 3, and 5 Shown in Fig. 6 (Weight Percent)

Slag	P-Enriched Phase	CaO	SiO ₂	MgO	Al ₂ O ₃	Fe ₂ O	P ₂ O ₅	TiO ₂
1	B1	54.11	19.64	2.45	2.71	3.17	17.92	0
3	B2	52.03	17.56	1.44	3.01	1.93	22.12	1.91
5	B3	47.66	16.03	1.78	0.91	2.11	30.17	1.34

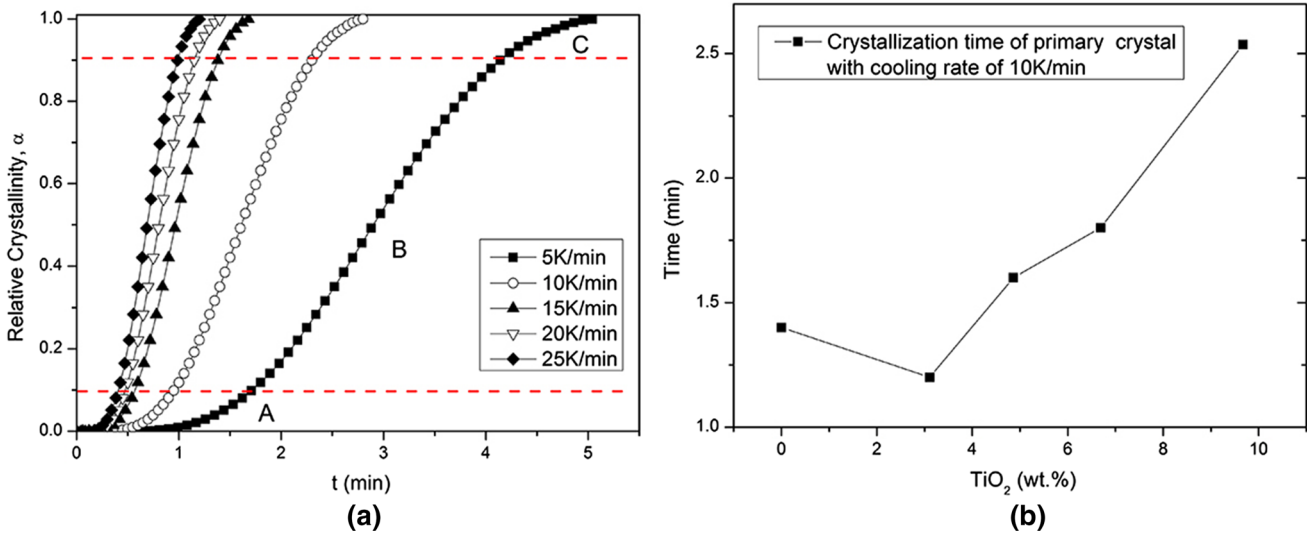


Fig. 7—(a) Relative crystallization as a function of time for slag 1 at five different cooling rates. (b) Crystallization time of primary crystals with the cooling rate of 10 K/min.

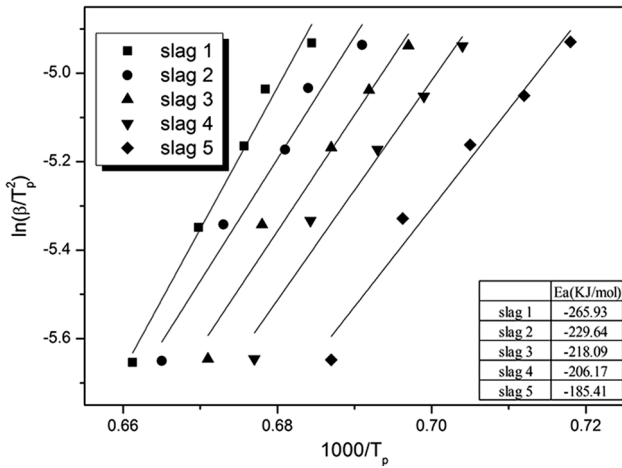
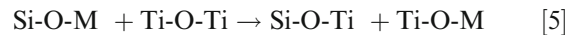
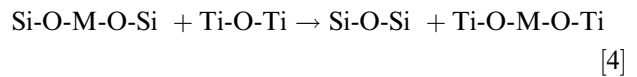


Fig. 8—Kissinger plot for determination of the activation energy (E_a) for exothermal reaction of the primary crystal from DSC with different cooling rates (5, 10, 15, 20, and 25 K/min).

vibration of the dominant P-related groups, *i.e.*, P-O-P and Si-O-P in the structure. The band near 680 cm⁻¹ can be assigned to the tetrahedrally coordinated Fe³⁺.^[25,26] By analogy with the spectroscopic results on the melts with others,^[31,45] the bands at about 790 and 845 cm⁻¹ can be assigned to Ti₂O₆⁴⁻ chain units and TiO₄⁴⁻ monomers (or Si-O-Ti) structural units, respectively. The band around 644 cm⁻¹ could be ascribed to Ti-O stretch vibration of Ti⁴⁺ in [TiO₆]-octahedra. Additionally, the band in the vicinity of 710 cm⁻¹

probably is due to O-Ti-O or O-(Si,Ti)-O deformation in chain or sheet units or both.^[45,46]

It can be found from the deconvoluted Raman spectra that with the increasing TiO₂ content, the Q² and Q³ bands gradually increase in intensity and become more distinct, whereas the intensity of Q⁰ and Q¹ bands decrease. It means the increasing degree of the polymerization (DOP) of the silicate structure. According to Mysen,^[47] the role of TiO₂ can compete with silicate complexes to coordinate metal cations (such as Ca²⁺). The competition process can be represented by the following reaction:^[45,46]



where M represents the metal cation. Therefore, some portion of the nonbridging oxygens in the silicate melts transformed into bridging oxygen with the addition of TiO₂, thereby polymerizing the portion of the silicate network, which can also be validated from the ²⁹Si NMR as shown in Figure 10. Furthermore, Ti⁴⁺ can substitute for Si⁴⁺ in tetrahedral coordination in the structural units in the structure, and the number of average bridging oxygen will be significantly larger. In this case, the DOP of the slags will be increased in theory.

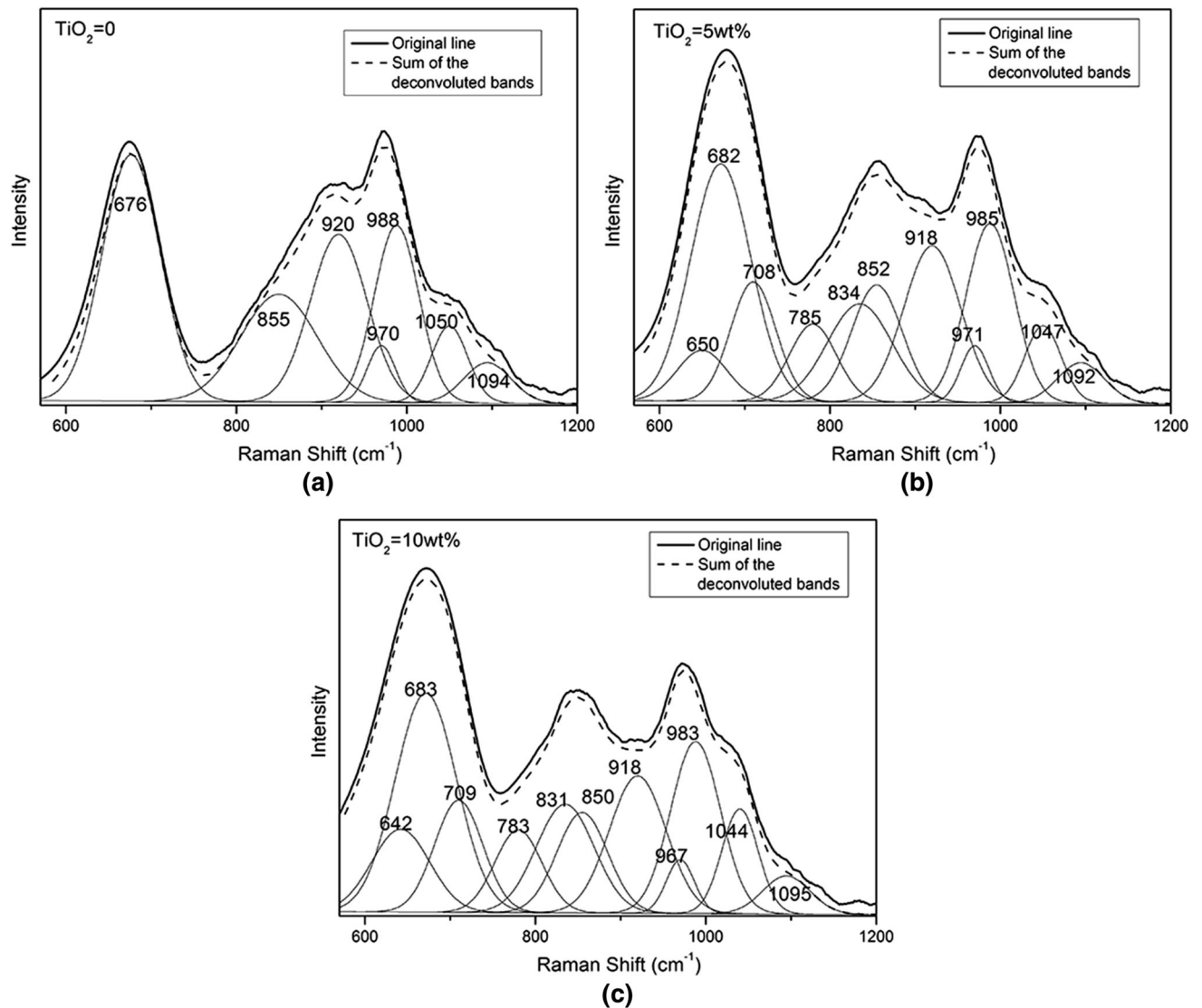


Fig. 9—Deconvoluted Raman spectra of CaO-SiO₂-MgO-Al₂O₃-FeO-P₂O₅-(TiO₂) slags with varying TiO₂ contents. (a) slag 1, (b) slag 3, and (c) slag 5.

Nevertheless, the physical properties of silicate melts such as viscosity are dependent on both the degree of polymerization and the strength of oxygen bridges in the silicate melts.^[45] The present structural study shows that the degree of polymerization is slightly enhanced with TiO₂ addition. Therefore, the decreasing viscosity could not be explained by the increasing DOP. According to Zhang *et al.*^[47,48] and Zheng *et al.*,^[31] the strength of Ti-O bonds seems to be much weaker than Si-O bonds for the reason that Ti⁴⁺ cation is larger in size and smaller in electronegativity compared with Si⁴⁺; thus, the addition of TiO₂ to highly polymerized melts will decrease the viscosity.

Additionally, from the viewpoint of the structure, the Ti-related bands could give a qualitative explanation to the change of crystal phases, especially to Mg₂TiO₄, CaTiO₃, and CaSiTiO₅. According to Grave^[49] and Ye,^[50] Ti⁴⁺ was octahedrally coordinated in Mg₂TiO₄. Harrison *et al.*^[38] investigated the cation ordering of MgFe₂O₄-Mg₂TiO₄ solid solution and found the

dominant chemical interaction of the solid solution was a positive nearest-neighbor pairwise interaction between tetrahedrally coordinated Fe³⁺ and octahedrally coordinated Ti⁴⁺. Therefore, [FeO₄]-tetrahedra and [TiO₆]-octahedra can co-polymerize to expedite the MgFe₂O₄-Mg₂TiO₄ solid solution formation, which has a lower crystallization temperature in thermodynamics. In addition, the [TiO₆]-octahedra structure unit is also the main component to build the structure of CaTiO₃.^[51] Therefore, CaTiO₃ was gradually crystallized. According to Li^[51] and Kirkpatrick,^[52] CaTiO₃ crystals were in nonfaceted morphology and the crystallization rate of CaTiO₃ rate was controlled by the diffusion of ion units (Ca²⁺ ion and octahedrally coordinated Ti⁴⁺ units) from bulk melts to the crystal-melt interface. In this case, the decreasing viscosity has a constructive effect on the crystallization of CaTiO₃. Moreover, the appearance of Ti-O-Si band characterized that the [TiO₄]-tetrahedra units can copolymerize with [SiO₄]-tetrahedra units to enhance the crystallization of CaSiTiO₅.

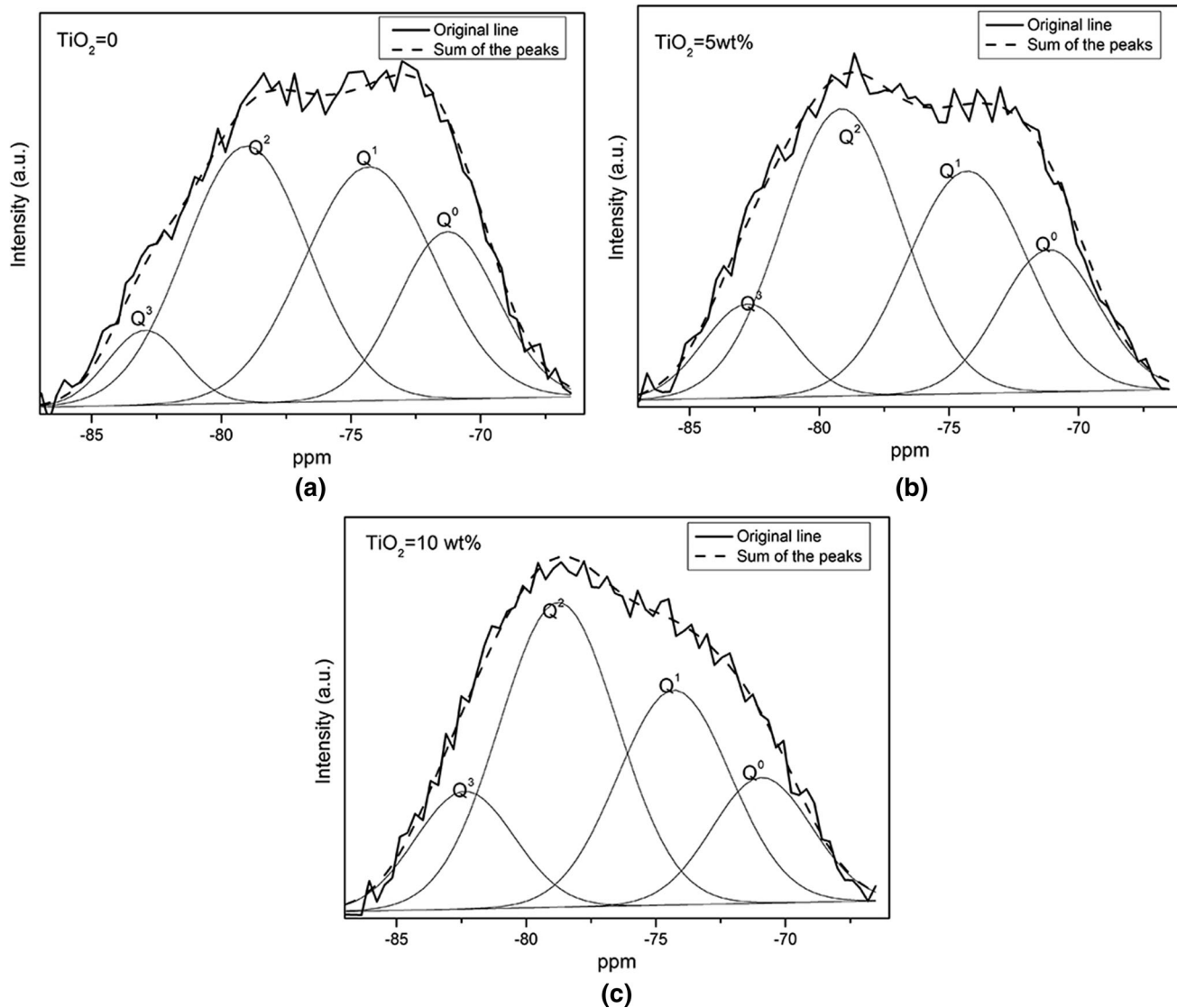


Fig. 10—Deconvoluted results of ^{29}Si MAS-NMR for slags with different TiO_2 contents. (a) slag 1, (b) slag 3, and (c) slag 5.

Combining the microstructure with the crystallization analysis, the primary enrichment mechanism of phosphorus may be elucidated. As chemical reaction in Eq. [1] shows, TiO_2 would capture C_2S (Ca^{2+} and $[\text{SiO}_4]$ units) from the early precipitated solution ($n\text{C}_2\text{S}-\text{C}_3\text{P}$) to form CaSiTiO_5 and CaTiO_3 ; *i.e.*, C_2S vanished gradually (which can also be clarified from the decreasing Q^0 unit in Raman and NMR spectra^[53]) and improved the concentration of phosphorus in the P-enriched phase, which is consistent with the results of XRD. Moreover, it can be found from Table II that the solid solubility of phosphorus in the P-enriched phase can reach a value as high as 30.17 wt pct, which can fully reach the phosphorus content requirements of phosphatic fertilizer for agriculture.

V. CONCLUSION

In the present study, the effect of TiO_2 on the viscous and crystallization behavior of P-bearing steelmaking slags was investigated. The results can be summarized as follows:

The viscosity of the slags decreased with increasing TiO_2 content, and the crystallization tendency decreased with the addition of TiO_2 . Additionally, an increasing TiO_2 content promotes the formation of $[\text{TiO}_6]$ -octahedra units, which are octahedrally coordinated in MgFe_2O_4 - Mg_2TiO_4 solid solution and CaTiO_3 . Moreover, $[\text{TiO}_4]$ -tetrahedra units can co-polymerize with $[\text{SiO}_4]$ -tetrahedra to form CaSiTiO_4 . It is meaningful to find that the formation of CaTiO_3 and CaSiTiO_4 was beneficial to the enrichment of phosphorus in the P-enriched phase, which enhanced the solid solubility of phosphorus in the P-enriched phase by removing units of $2\text{CaO}\cdot\text{SiO}_2$ and, thus, increasing the P-content in $n2\text{CaO}\cdot\text{SiO}_2-3\text{CaO}\cdot\text{P}_2\text{O}_5$.

ACKNOWLEDGMENTS

Support from the National Natural Science Foundation of China (51522401, 51472007, 51372019) and the National High Technology Research and Development

Program of China (863 Program, 2012AA06A114) is acknowledged.

REFERENCES

1. World Steel Association: <https://www.worldsteel.org/media-centre/press-releases/2015/World-crude-steel-output-increases-by-1.2-in-2014.html>.
2. B. Das, S. Prakash, P. Reddy, and V. Misra: *Resour. Conserv. Recy.*, 2007, vol. 50, pp. 40–57.
3. M. Shi, Q. Wang, and Z. Zhou: *Constr. Build. Mater.*, 2015, vol. 98, pp. 649–55.
4. Q. Wang, M. Shi, and Z. Zhang: *J. Therm. Anal. Calorim.*, 2015, vol. 120, pp. 1241–48.
5. P. Yan, G. Mi, and Q. Wang: *J. Therm. Anal. Calorim.*, 2014, vol. 115, pp. 193–200.
6. Q. Wang, J. Yang, and P. Yan: *Powder Technol.*, 2013, vol. 245, pp. 35–39.
7. Q. Wang, P. Yan, and J. Yang: *Constr. Build. Mater.*, 2013, vol. 47, pp. 1414–20.
8. J. Jun: *Min. Metall.*, 2003, vol. 12, pp. 33–37.
9. L. Lin, Y.P. Bao, M. Wang, and H.M. Zhou: *Ironmak. Steelmak.*, 2014, vol. 41, pp. 193–98.
10. L. Lin, Y.P. Bao, M. Wang, W. Jiang, and H.M. Zhou: *J. Iron Steel Res. Int.*, 2014, vol. 21, pp. 496–502.
11. M.Y. Wang, L.N. Zhang, L. Zhang, Z.T. Sui, and G.F. Tu: *Trans. Nonferrous Met. Soc. China*, 2006, vol. 16, pp. 421–25.
12. X.R. Wu, J.N. An, R.H. Chen, and L.S. Li: *J. Anhui Univ. Tech.*, 2010, vol. 27, pp. 233–37.
13. Y.Q. Sun, J. Li, X.D. Wang, and Z.T. Zhang: *Metall. Mater. Trans. B*, 2014, vol. 45B, pp. 1446–55.
14. G. Kor: *Metall. Trans. B*, 1977, vol. 8, pp. 107–13.
15. H. Suito and R. Inoue: *Trans. ISIJ*, 1982, vol. 22, pp. 869–77.
16. J. Berak and I. Tomczakh: *Roczniki Chemii*, 1972, vol. 46, pp. 2157–64.
17. H. Ono, A. Inagaki, T. Masui, H. Narita, S. Nosaka, T. Mitsuo, and S. Gohda: *Trans. ISIJ*, 1981, vol. 21, pp. 135–44.
18. L. Lin, Y.P. Bao, Q. Yang, M. Wang, and W. Jiang: *Ironmak. Steelmak.*, 2015, vol. 42, pp. 331–38.
19. L. Lin, Y.P. Bao, M. Wang, and H.M. Zhou: *J. Univ. Sci. Technol. Beijing*, 2014, vol. 36, pp. 1013–19.
20. L. Jiang, J. Diao, X. Yan, B. Xie, Y. Ren, T. Zhang, and G. Fan: *ISIJ Int.*, 2015, vol. 55, pp. 564–69.
21. J. Diao, B. Xie, Y.H. Wang, and X. Guo: *ISIJ Int.*, 2010, vol. 50, pp. 768–70.
22. Z.J. Wang, Y.Q. Sun, S. Sridhar, M. Zhang, M. Guo, and Z.T. Zhang: *Metall. Mater. Trans. B*, 2015, vol. 46B, pp. 537–41.
23. Z.J. Wang, Y.Q. Sun, S. Sridhar, M. Zhang, M. Guo, and Z.T. Zhang: *Metall. Mater. Trans. B*, 2015, vol. 46B, pp. 2246–54.
24. Z.J. Wang, Y.Q. Sun, S. Sridhar, M. Zhang, M. Guo, Z.M. Li, Z.C. Guo, and Z.T. Zhang: *ISIJ Int.*, 2016, vol. 56, pp. 546–53.
25. Z.J. Wang, Q.F. Shu, S. Sridhar, M. Zhang, M. Guo, and Z.T. Zhang: *Metall. Mater. Trans. B*, 2015, vol. 46B, pp. 758–65.
26. S.S. Jung and I. Sohn: *Environ. Sci. Technol.*, 2014, vol. 48, pp. 1886–92.
27. Y.B. Cheng, C. Xu, S.Y. Pan, Y.F. Xia, R.C. Liu, and S.X. Wang: *J. Non-Cryst. Solids*, 1986, vol. 80, pp. 201–08.
28. A. Tilocca and A.N. Cormack: *J. Phys. Chem. B*, 2007, vol. 111, pp. 14256–64.
29. J.L. Li, Q.F. Shu, and K.C. Chou: *ISIJ Int.*, 2014, vol. 54, pp. 721–27.
30. L.S. Li, X.R. Wu, L. Yu, and Y.C. Dong: *Ironmak. Steelmak.*, 2008, vol. 35, pp. 367–70.
31. K. Zheng, Z.T. Zhang, L.L. Liu, and X.D. Wang: *Metall. Mater. Trans. B*, 2014, vol. 45B, pp. 1–9.
32. H. Park, J.Y. Park, G.H. Kim, and I. Sohn: *Steel Res. Int.*, 2012, vol. 83, pp. 150–56.
33. Z. Wang, Q.F. Shu, and K.C. Chou: *Steel Res. Int.*, 2013, vol. 84, pp. 766–76.
34. M.D. Seo, C.B. Shi, J.W. Cho, and S.H. Kim: *Metall. Mater. Trans. B*, 2014, vol. 45B, pp. 1874–86.
35. G.H. Wen, S. Sridhar, P. Tang, X. Qi, and Y.Q. Liu: *ISIJ Int.*, 2007, vol. 47, pp. 1117–25.
36. V.D. Eisenhüttenleute: *Slag atlas*. Verlag Stahleisen, 1995.
37. S. Fukagai, T. Hamano, and F. Tsukihashi: *ISIJ Int.*, 2007, vol. 47, pp. 187–89.
38. R.J. Harrison, E.J. Palin, and N. Perks: *Am. Mineral.*, 2013, vol. 98, pp. 698–708.
39. H.E. Kissinger: *J. Res. Natl. Bur. Stand.*, 1956, vol. 57, pp. 217–21.
40. T. Ozawa: *Polymer*, 1971, vol. 12, pp. 150–58.
41. S. Haratian and M. Haddadsabzevar: *J. Non-Cryst. Solids*, 2015, vol. 429, pp. 164–70.
42. P. Supaphol, N. Dangeeeyun, P. Srimoanon, and M. Nithitanakul: *Thermochim. Acta*, 2003, vol. 406, pp. 207–20.
43. M. Dapiaggi, G. Artioli, C. Righi, and R. Carli: *J. Non-Cryst.*, 2007, vol. 353, pp. 2852–60.
44. B.O. Mysen, L.W. Finger, D. Virgo, and F.A. Seifert: *Am. Mineral.*, 1982, vol. 67, pp. 686–95.
45. B.O. Mysen: *Am. Mineral.*, 1980, vol. 65, pp. 1150–65.
46. S.F. Zhang, X. Zhang, C.G. Bai, L.Y. Wen, and X.W. Lv: *ISIJ Int.*, 2013, vol. 53, pp. 1131–37.
47. L. Zhang and S. Jahanshahi: *The Seventh International Conference on Molten Slags, Fluxes and Salts*, South African Institute of Mining and Metallurgy, Johannesburg, South Africa, 2004, pp. 51–6.
48. B.O. Mysen, F.J. Ryerson, and D. Virgo: *Am. Mineral.*, 1980, vol. 65, pp. 1150–65.
49. E.D. Grave, J.D. Sitter, and R. Vandenbergh: *Appl. Phys.*, 1975, vol. 7, pp. 77–80.
50. T. Ye, S. Li, X. Wu, M. Xu, X. Wei, K. Wang, H. Bao, J. Wang, and J. Chen: *J. Mater. Chem. C*, 2013, vol. 1, pp. 4327–33.
51. J.L. Li, Q.F. Shu, X.M. Hou, and K.C. Chou: *ISIJ Int.*, 2015, vol. 55, pp. 830–36.
52. R.J. Kirkpatrick: *Am. Mineral.*, 1975, vol. 60, pp. 798–814.
53. K. Mills, L. Yuan, and R. Jones: *J. S. Afr. Inst. Min. Metall.*, 2011, vol. 111, pp. 649–58.